LIMNOLOGY and OCEANOGRAPHY

ASLO

Limnol. Oceanogr. 9999, 2022, 1–16

doi: 10.1002/lno.12169

Copepod interaction with small-scale, dissipative eddies in turbulence: Comparison among three marine species

Dorsa Elmi,[1] Donald R. Webster ,[1*] David M. Fields [2]

[1]School of Civil and Environmental Engineering, Georgia Institute of Technology, Atlanta, Georgia
[2]Bigelow Laboratory for Ocean Sciences, East Boothbay, Maine

Abstract

A physical model of a Burgers vortex was created in the laboratory with characteristics corresponding to dissipative-scale eddies that copepods are likely to encounter in turbulent flows. The swimming behavior of three marine copepod species is assessed as a function of vortex strength in and around the flow structure with the vortex axis aligned vertically or horizontally in the water. The studied species are *Acartia tonsa*, an estuarine copepod with a hop-sink swimming style; *Temora longicornis*, a coastal copepod with a cruise swimming style; and *Calanus finmarchicus*, an open-ocean copepod with a cruise-sink swimming style. The results show that copepods change their swimming behavior with the intensity of the Burgers vortex and reveal species-specific responses in nearly all kinematic parameters. *A. tonsa* and *C. finmarchicus* exhibited the strongest behavioral response to increasing vortex strength and *T. longicornis* exhibited the weakest response. *A. tonsa* and *T. longicornis* showed no response to changes in vortex orientation, whereas the behavior of *C. finmarchicus* revealed some vortex orientation dependence. One common behavior among the species is that the swimming trajectory shape becomes increasingly curved and spiral around the vortex core with increasing vortex strength, which provides a means of local aggregation and increased encounter rate with food and mates. The results are interpreted in relation to differences in swimming style and setal morphology among the species.

Copepods, a group of small (0.1–10 mm) aquatic crustaceans, are a highly abundant metazoan in the oceans and a critical link in the marine food web, bridging the gap between primary producers and higher trophic levels such as fish and mammals, including whales (Beaugrand et al. 2003; Turner 2004; Castonguay et al. 2008). Ocean turbulence modulates individual behavior of copepods (Marrasé et al. 1990; Visser et al. 2001) and influences the distribution of species within the water column (Haury et al. 1990; Mackas et al. 1993; Incze et al. 2001). Species-specific responses to turbulence can alter zooplankton community structure and potentially affect the predator–prey interactions that rely on these encounters (Yamazaki 1993; Saiz 1994; Michalec et al. 2017).

Turbulence intensity varies over time and space in the upper ocean layer with significant variation in the vertical direction. Observations have shown that spatial distributions of copepods are highly dependent on the level of turbulence they experience (Incze et al. 2001; Visser et al. 2001). Incze et al. (2001), in particular, compared the vertical distribution of copepod species before and after the passage of a storm. *Calanus finmarchicus* and *Temora* spp. migrated vertically downward to deeper layers where the water is less turbulent. Similarly, horizontal variations of turbulence intensity over different regions of the ocean (e.g., estuaries vs. open ocean) can change with copepods' proximity to the coast (Manning and Bucklin 2005).

At the scale of copepods, turbulent fluid motion consists of eddy structures that present as small worm-like vortices with varying strength and orientation (Vincent and Meneguzzi 1991). The size of the vortical structures in the dissipative range, as well as the size of copepods, is similar to the Kolmogorov microscale ($\eta \sim$ 0.2–6 mm) (Jumars et al. 2009). The ability of copepods to detect and respond to this hydrodynamic landscape depends on the function of their sensory structure (setae). Yen et al. (1992) showed that copepods can detect setal displacements as small as 10 nm. However, the threshold fluid disturbance needed for behavior responses varies among species and developmental stages (Woodson et al. 2014). *Acartia tonsa* adults are comparatively sensitive to velocity gradients and escape in response to fluid strain rate, whereas nauplii require nearly an order of magnitude greater

*Correspondence: dwebster@ce.gatech.edu

Additional Supporting Information may be found in the online version of this article.

Author Contribution Statement: Conceptualization: D.E., D.R.W., D. M.F.; Methodology: D.E., D.R.W., D.M.F.; Software: D.E.; Validation: D.E.; Formal analysis: D.E., D.R.W., D.M.F.; Resources: D.M.F.; Data curation: D.E.; Writing – original draft: D.E., D.R.W., D.M.F.; Writing – review & editing: D.E., D.R.W., D.M.F.; Supervision: D.R.W.; Project administration: D.R.W., D.M.F.; Funding acquisition: D.R.W., D.M.F.

strain rate to evoke an escape (Fields and Yen 1997; Kiørboe et al. 1999). Furthermore, mechanosensitive copepods such as *A. tonsa* show rapid responses to hydrodynamic stimuli (Bagøien and Kiørboe 2005), whereas chemosensitive copepods, such as *Temora longicornis*, are less responsive to hydrodynamic signals (Burdick et al. 2007; Waggett and Buskey 2007).

Turbulence has been shown to influence metabolic rates, predator–prey encounter rates, grazing rates, egg production, swimming behavior, and population dynamics of marine zooplankton (Alcaraz and Saiz 1992; Saiz et al. 1992; Fields and Yen 1997). However, the response of copepods to characteristic features within an individual small-scale turbulent eddy is much less known. Recently, Elmi et al. (2021) showed that one copepod species (*A. tonsa*) can detect and respond to hydrodynamic features created in a Burgers vortex, the flow structure of which is consistent with the characteristics of dissipative-scale eddies in turbulence. The results suggest that the behavior of *A. tonsa* to the fluid motion within the dissipative-scale turbulent eddies drive the biological and ecological effects of turbulence.

This study hypothesizes that copepod species have different behavioral responses to the magnitude and orientation of small-scale turbulent eddies. There is limited understanding of the connection between the sensory organ morphology and swimming mode of copepods and their response to the fine-scale eddies created by turbulence. This study uses three marine copepod species, *T. longicornis* and *C. finmarchicus*, plus the previously reported *A. tonsa*, each having unique mechanosensory hair architecture and swimming mode (Table 1). Quantifying species-specific responses to oceanic turbulence is important for understanding the role of sensory structures in governing copepod behavior and for addressing regional patchiness of copepods. In an earlier study, Webster et al. (2015) reported that the responses of *A. tonsa* and *T. longicornis* to a moderately intense dissipation-scale vortex were different and suggested that the sensitivity of *A. tonsa* to turbulent features is related to the three-dimensional distribution of setae on the copepod's antennule. In this study, the two additional species, beyond *A. tonsa* reported in Elmi et al. (2021), represent a small (~ 1 mm) nearshore coastal copepod species (*T. longicornis*) and a large (2.5 mm) oceanic copepod (*C. finmarchicus*), each with a unique antennule architecture and swimming mode (Fig. 1; Table 1). The vortex structure is generated based on levels of turbulence that copepods experience in their habitats. Furthermore, to investigate the directional response of the copepod species to the hydrodynamics of small-scale eddies, the Burgers vortex stimulus is generated in horizontal and vertical orientations.

Materials

Laboratory experiments were conducted to observe the swimming behavior of three copepod species in the vicinity of a Burgers vortex. The experimental setup and flow measurement technique are described in detail in Elmi et al. (2021) and briefly included here.

Small-scale dissipative eddies in the laboratory

Jumars et al. (2009) introduced a new approach to examine turbulence–plankton interaction. The idea is to reduce the stochastically varying nature of turbulent flows to a simple vortex model. Such an approach has the advantage of eliminating the time-varying and random nature of the flow, and the approach facilitates examination of the mechanistic aspects of plankton interaction with a dissipation-scale eddy. In the current study, isolated Burgers vortices were generated in the laboratory to simulate a dissipative-scale turbulent eddy that copepods encounter in their habitats.

Jumars et al. (2009) report that the Burgers vortex is a good model for turbulent vortices at the scale of the plankton. The Burgers vortex is named for the Burgers (1948) analytical solution of the Navier–Stokes equations. The velocity components are described (in cylindrical coordinates, $r-\theta-x$) by:

$$u_r = -ar \qquad u_\theta = \frac{\Gamma}{2\pi r}\left[1 - e^{\frac{-r^2 a}{2\nu}}\right] \qquad u_x = 2ax, \qquad (1)$$

where a is the axial strain rate and Γ is the vortex circulation. As shown in Fig. 2, the flow consists of a rotating motion around the center axis (Fig. 2a) while the fluid is being stretch in the axial direction (Fig. 2d). The velocity, vorticity, and strain rate fields are axisymmetric (i.e., independent of the θ coordinate). Furthermore, the dashed line shown in Fig. 2 identifies the characteristic vortex radius, defined as $r_B = \sqrt{\frac{2\nu}{a}}$.

The apparatus to create the vortex treatment in the laboratory consisted of two co-axial disks rotating at the same rate inducing rotation of the fluid between them (Webster and Young 2015; Elmi et al. 2021). Simultaneously, water was drawn into the center of the disks to create a balance between radially outward diffusion and inward advection of vorticity. Turbulence at the scale of copepods is isotropic, which implies that copepods encounter dissipative eddies in random

Table 1. Characteristics of the three marine copepod species.

Species	Setal array morphology	Swimming orientation	Swimming style	Habitat
Acartia tonsa	Distributed around the antennule	Mostly vertical	Hop-Sink	Estuarine
Temora longicornis	Planar array	Mostly horizontal	Cruising	Coastal
Calanus finmarchicus	Planar array	Vertical	Cruise-sink	Open ocean

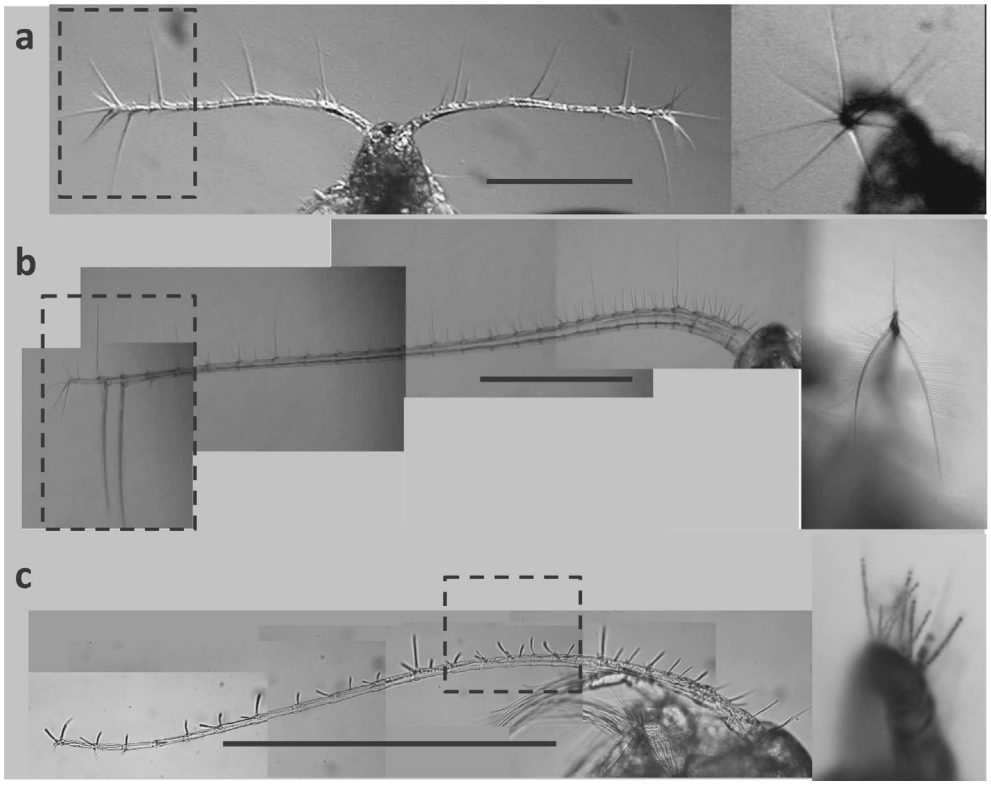

Fig. 1. Setal architecture of three copepod species. The scale bar length corresponds to 500 μm. The dorsal view is shown on the left, and the dashed box shows the location of the orthogonal view of the antennule shown on the right. (**a**) *Acartia tonsa*: the left image shows setae oriented in all directions (Fields 2014). The right image is an end view of the antennule, (**b**) *Calanus finmarchicus*: the left image shows that antennules are furnished with a planar distribution of setae with long hairs at the distal tip. The right image is the end view of the antennule (Fields 2014), and (**c**) *Temora longicornis*: antennules are furnished with a planar distribution of setae. The right image is an end view of a mid-region of the antennule.

directions (for a visualization of the turbulent eddy flow structure, *see* Yokokawa et al. 2002). To examine directional response of copepods to vortical structures, a Burgers vortex was generated (separately) with the vortex axis aligned with the horizontal and vertical orientations.

The flow structure of a Burgers vortex provides a suite of potential hydrodynamic cues for the copepods, such as vorticity and shear strain rate, that are spatially separated within the vortex (Jumars et al. 2009; Webster and Young 2015; Elmi et al. 2021). As seen in Figs. 2b, 3a, the vorticity, ω_x, is maximum at the vortex axis and decreases with radial distance. The vorticity is generally small at locations outside of the characteristic vortex radius, hence it is helpful to think of most of the fluid rotation occurring in the core of the vortex at radial locations smaller than r_B. The shear strain rate, $e_{r\theta}$, reaches a local maximum value for a radial location slightly greater than r_B and equals zero both at the center axis and at large radial distances (Figs. 2c, 3b). As the vortex intensity increases, the vortex radius shrinks and the maximum vorticity and shear strain rate increase (Fig. 3; Table 2). The axial strain rate ($a = \frac{1}{2}\frac{\partial u_x}{\partial x}$), that is, stretching of the vortex, also increases as the strength of the vortex increases as indicated by the variation in slope of the profiles in Fig. 3c and quantified in Table 2.

In this study, the vortex was generated to correspond to four turbulent intensities as defined in Webster et al. (2004) and a control level consisting of stagnant fluid. The range of dissipation rate (Table 2) corresponded to the turbulence intensity of open ocean, coastal zones, and estuaries, inhabited by *C. finmarchicus*, *T. longicornis*, and *A. tonsa*, respectively. The Burgers vortex generated corresponded to the eddy size for the median dissipation rate for each of the targeted turbulent conditions, in order to present a "typical" vortex structure (Jumars et al. 2009). Specifically, Jumars et al. (2009) argue that a "typical vortex" is represented by the scale of the median dissipation rate (i.e., the scale at which half of the dissipation rate occurs above that scale, and half occurs below). Therefore, the scale that corresponds to a characteristic radius, r_B, of a dissipative vortex is 8.1η, where η is the Kolmogorov microscale (Jumars et al. 2009; Webster and Young 2015).

The velocity field in this complex three-dimensional flow was quantified using the tomographic particle image velocity (PIV) technique (technique description in Murphy et al. 2012). The flow measurements used four high-resolution synchronized cameras (Phantom v210, 1280 $\times$ 800 pixels, with 105-mm lenses) and 20-μm tracer particles (Murphy et al. 2012; Elmi et al. 2021). Tracer particles were illuminated

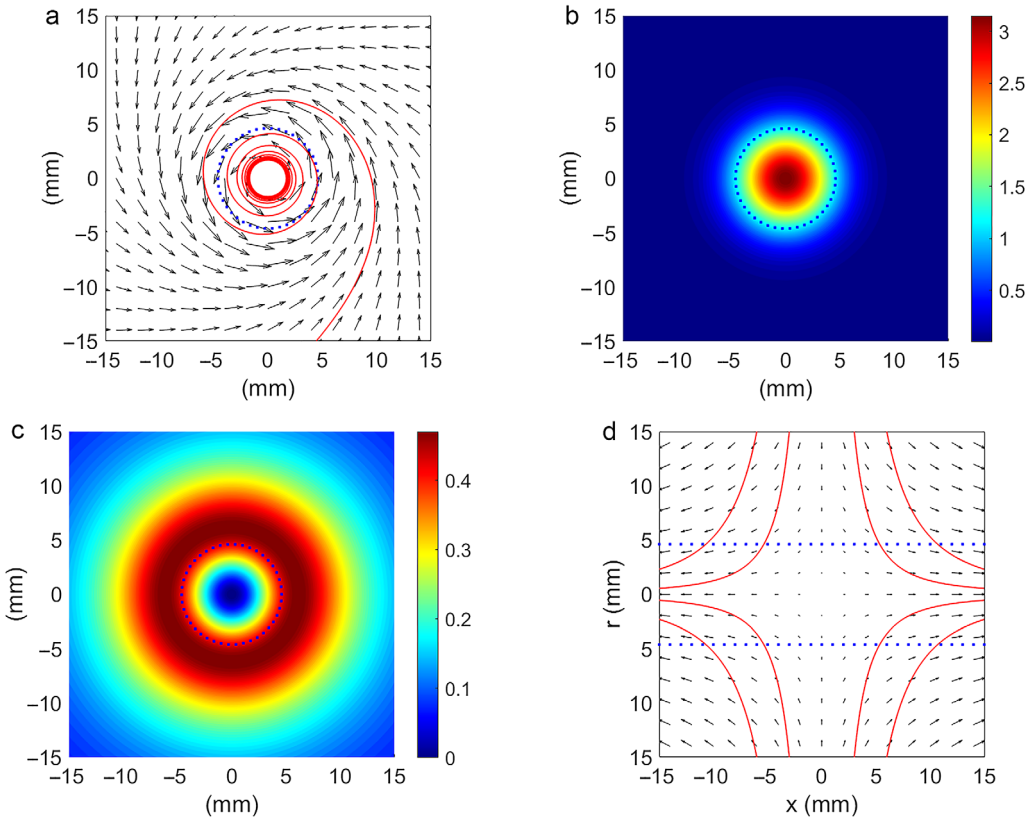

Fig. 2. (**a**) Velocity, (**b**) vorticity ω_x (s^{-1}), and (**c**) shear strain rate $|e_{r\theta}|$ (s^{-1}) fields shown in the r-θ plane, and (**d**) velocity field in the r-x plane for a theoretical Burgers vortex. For example purposes, the parameters are $\Gamma = 2.15$ cm^2 s^{-1} and $a = 0.093$ s^{-1}, which correspond to a level 3 vortex (Table 2). The dashed circle (**a**–**c**) and lines (**d**) indicate the characteristic vortex radius, r_B. Also shown in (**a**) and (**d**) are example streamlines (the red curves projected onto the plotted plane), which combine to form a three-dimensional spiral.

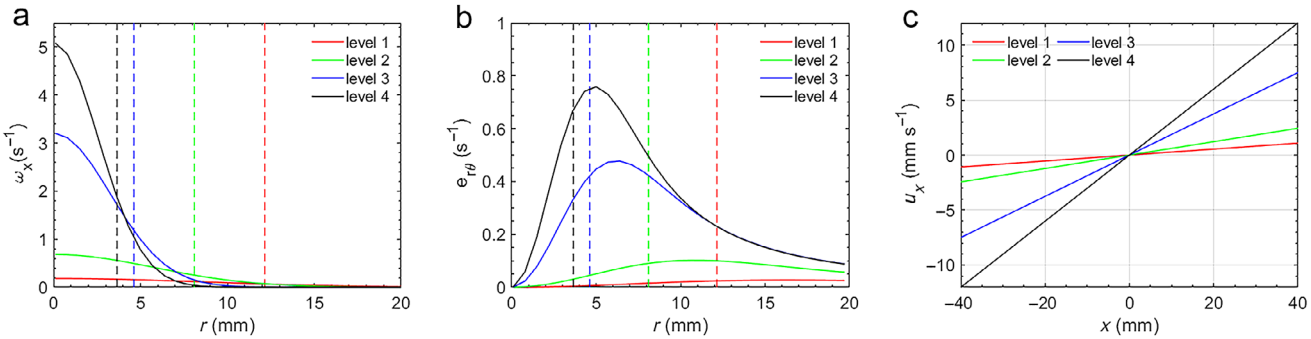

Fig. 3. (**a**) Radial profiles of vorticity, ω_x, (**b**) radial profiles of shear strain rate, $|e_{r\theta}|$, and (**c**) axial profiles of the axial velocity component, u_x, for the Burgers vortex for four vortex strengths: (black) level 4, (blue) level 3, (green) level 2, (red) level 1. The vortex strength levels were defined by measurements in the isotropic turbulence apparatus described by Webster et al. (2004) and all parameters are defined in Table 2. The vertical dashed line indicates the characteristic radius of the vortex (r_B), which gets smaller for increasing vortex intensity.

with infrared lasers (808 nm wavelength). Measurements were carried out in an 3 cm × 3 cm × 3 cm observation volume between the disks in the middle of the experimental tank (20.6 cm × 20.6 cm × 27.3 cm, horizontal apparatus; 25.4 cm × 25.4 cm × 27.9 cm, vertical apparatus). The tomographic PIV flow analysis was conducted in the DaVis software (LaVision Inc.) using the MART algorithm and cross-correlation technique (Elmi et al. 2021).

The Burgers vortex apparatus was designed with adjustable parameters such as water flow rate into the hollow shafts, rotation speed of the disks, and the distance between the disks (Elmi et al. 2021). Changing these apparatus parameters

Table 2. Burgers vortex parameters for each vortex intensity level. The corresponding turbulent dissipation rate, ε, and Kolmogorov length scale, η, are from Webster et al. (2004).

Vortex intensity level	1	2	3	4
Target ε (cm^2s^{-3})	0.002	0.009	0.096	0.25
Target η (cm)	0.15	0.1	0.057	0.045
Target r_B (cm)	1.21	0.81	0.46	0.36
Target axial strain rate, a (s^{-1})	0.014	0.030	0.093	0.15
Target circulation, Γ (cm^2s^{-1})	0.84	1.41	2.15	2.13
Horizontal treatment				
Measured axial strain rate, a (s^{-1})	0.014	0.025	0.1	0.14
Measured circulation, Γ (cm^2s^{-1})	0.92	1.70	2.52	2.45
Vertical treatment				
Measured axial strain rate, a (s^{-1})	0.015	0.028	0.092	0.143
Measured circulation, Γ (cm^2s^{-1})	0.89	1.43	2.58	2.39

r_B, characteristic radius of the vortex; a, axial strain rate; Γ, circulation.

facilitated generating the target vortex characteristics. Example measured fields of the velocity and the axial component of vorticity, in this case for the level 3 vortex treatment with vertical alignment of the vortex axis, are provided in the Supporting Information (Fig. S1). The study measured the main characteristics of the vortex, that is, axial strain rate (a) and circulation (Γ), and compared them to the target parameters defined by the turbulent flow conditions reported in Webster et al. (2004). Axial strain rate is defined above and the circulation is a measure of the total fluid rotation in the vortex and is obtained from the surface integral of vorticity, $\Gamma = \int\int \omega_x \cdot dA$. The reconstructed velocity fields validated that the intensity of the generated vortex in the experiments was comparable to the target turbulence characteristics at the scale of copepods (Table 2). Table 2 also reports the target turbulence conditions as well as the characteristic radius of the vortex, r_B.

Copepod collection and maintenance

The selected copepods, *A. tonsa*, *T. longicornis*, and *C. finmarchicus*, are endemic to regions with different levels of turbulence (Kiørboe and Saiz 1995; Saiz and Kiørboe 1995; Fields and Yen 1997). Furthermore, they use different swimming modes and have distinct antennule architectures (Table 1). *A. tonsa* occupies highly energetic environments found in the upper water column (above the thermocline) in coastal waters. *A. tonsa* is a hop-sink swimmer and swims mostly in a vertical direction. Sensory setae of *A. tonsa* are oriented in three dimensions all around the antennules (Fig. 1a). *T. longicornis* also occupies coastal regions, but is generally located in calmer bays, in part to facilitate its mate tracking behavior. *T. longicornis* is a smooth swimmer and moves mostly in a horizontal plane in the water. The setae form a planar array on the antennules of *T. longicornis* (Fig. 1c). *C. finmarchicus* is a large, open-ocean copepod that lives below the thermocline. *C. finmarchicus* is a diel vertical migrator that can cover hundreds of meters per day. The copepod moves through a series of repetitive hops followed by a short sinking period. Its antennules have a planar array of setae with a few long hairs at the distal end (Fig. 1b). *C. finmarchicus* swims mainly with a vertical body orientation in the water. *C. finmarchicus* and *T. longicornis* were captured in vertical net tows (75 cm diameter, 333 μm mesh) near Bigelow Laboratory for Ocean Sciences in East Boothbay, Maine, USA using a sealed cod end to maintain healthy specimens with their setal array fully intact. *C. finmarchicus* was collected ~ 5 nautical miles from shore in ~ 110 m of water. *T. longicornis* was collected within a small bay adjacent to the lab in ~ 20 m of water. Post-collection, animals were transported to the lab and maintained at 13°C on a mixed diet of the diatom *Thalassiosira weissflogii* (CCMP # 1336) and the cryptophyte *Rhodomonas salina* (CCMP # 1319). Copepods were held for less than 2 weeks prior to use. *A. tonsa* were reared in culture at the Bigelow Laboratory for Ocean Sciences. Populations of mixed-sex adult specimens were shipped to the Georgia Institute of Technology in Atlanta, GA, USA in thermally insulated containers.

Copepod behavioral analysis

Experiments were conducted in a temperature-controlled room at 13°C and the water salinity level was maintained at 33 Practical Salinity Unit (PSU). Roughly 300 (*A. tonsa* and *T. longicornis*) or 100 (*C. finmarchicus*) individuals were introduced gently into the tank for each trial, which created a low population density to minimize the potential interactions (which were rarely observed). Digital recordings were made in a dark room to avoid behavioral response to changes in light (Fields et al. 2012). Prior to the experiment, copepods were fed the cryptophyte *R. salina* (10^4–10^5 cells mL^{-1}; CCMP # 1319). Two high-resolution cameras recorded the motion of copepods inside the vortex volume from orthogonal perspectives. Video recording started with a 15-min delay to allow the vortex flow to become stable, and the behavior observations were performed independently of the flow measurements described above. Trajectories were tracked manually using the DLTdv5 package for MATLAB (Hedrick 2008). For *C. finmarchicus*, head and tail points were tracked separately to investigate the changes in the body orientation of copepods with respect to the vortex axis and gravity. Three-dimensional trajectories were generated by matching the two-dimensional trajectories from each perspective using a self-developed MATLAB code. Three-dimensional trajectories were overlaid on the vortex volume to calculate swimming kinematic variables. The experiments were repeated with three unique populations for each copepod species. For each population, four vortex treatments and a stagnant control treatment were recording in a random sequence. The experiments were conducted for horizontal and vertical treatments with different populations of

copepods. The sample size is reported in Supporting Information (Table S1).

The three-dimensional swimming paths of copepods were characterized by a variety of measures, including relative velocity, net-to-gross-displacement ratio (NGDR), fractal dimension, turn frequency, jumping frequency and acceleration, proportional residence time inside the vortex, and trajectory angle with respect to the flow. Relative velocity is defined as the copepod total velocity vector minus the local fluid velocity vector. NGDR is a measure of linearity of trajectories and has values between 0 and 1. Large NGDR values correspond to straight trajectories and values close to 0 correspond to loopy trajectories. NGDR is a scale-dependent variable and depends on the length of the trajectory (Tiselius 1992). Fractal dimension of the trajectory was calculated using a two-dimensional box counting algorithm that counts the number of boxes occupied by the trajectory (Seuront et al. 2004) in the $r-\theta$ plane perpendicular to the vortex axis. Fractal dimension increases with complexity of the trajectory. In this study, NGDR and fractal dimension were calculated for trajectories of 20-s duration to avoid scale-dependent results. Turn frequency was defined as the number of turns in the copepod trajectory greater than 20° that a copepod performs in 1 s.

Copepods perform two types of jumps. Hops are weak jumps and involve a single motion of the swimming legs. Escapes involve multiple cycles of the swimming legs, have greater acceleration rates, and propel the animal a greater distance (Fields 2000). While these behaviors can produce a continuum of speeds and accelerations, based on video observation, this study differentiated hop and escape jumps by defining a threshold acceleration of 70 $\mathrm{cm\,s^{-2}}$, with hops corresponding to acceleration events falling below this threshold. Furthermore, coordinated jumps related to mating events (observed in *A. tonsa* only) were omitted from the data.

Jump density was calculated to find the hydrodynamic cue triggering behavioral changes. Jump density ($\mathrm{jumps\,mm^{-2}\,s^{-1}}$), is defined as the number of jumps per time in an area of a circular bin ($A=\pi\left[(r+\Delta r)^2-r^2\right)], \Delta r=1\,\mathrm{mm}$) around the vortex axis. Because peak regions of the hydrodynamic cues of the Burgers vortex were located at different radial locations, jump density vs. vortex radius reveals the association of a particular hydrodynamic cue to the location of the jumps. Peak jump density at the vortex core would correspond to the location of maximum vorticity, whereas peak jump density near the vortex characteristic radius would correspond to the location of maximum shear strain rate.

Statistical analysis

The purpose of the statistical analysis was to evaluate the relationship between the kinematic parameters and the copepod species, vortex orientation, and the vortex strength (as quantified by the axial strain rate parameter). Statistical analysis was performed using a multivariate ANOVA followed by regression analysis for effects found to be significant. Three-way ANOVA analysis was used to assess the effect of axial strain rate, vortex orientation, and copepod species on the swimming response to Burgers vortex, and whether these variables interact with each other. Variables that were not normally distributed were transformed. Three-way ANOVA results are reported in the form of *F*-stat, degrees of freedom (dF), and significance level (*p*-value). A significance was indicated for $p < 0.05$. For variables with a significant effect of vortex strength in the ANOVA analysis, the correlation between the mean variables and the axial strain rate (representing vortex strength) was investigated using regression analysis. The slope of the regression line estimated the significance of the copepod's response to vortex strength. If the significance coefficient (p) is less than 0.05, the slope of the regression, and hence the response of the copepod to vortex strength, is significant. The kinematic variables that did not depend on vortex orientation were pooled for horizontal and vertical treatments.

Results

All three species of copepods showed distinct responses to the Burgers vortex. The responses were significantly different for species in all of the kinematic variables measured, except for the proportion of spiral trajectories ($p = 0.069$) (Table 3; three-way ANOVA). The results indicated that the complexity of swimming paths increased with vortex strength for *A. tonsa*, *T. longicornis*, and *C. finmarchicus* (Fig. 4 and *see* fig. 4 in Elmi et al. 2021 for *A. tonsa* trajectories). In still water and the level 1 vortex, relatively straight trajectories were the most common swimming paths for each species. With increased vortex strength, the trajectories became more aligned with the flow, resulting in a higher proportion (i.e., the fraction of total trajectories) of spiral trajectories around the vortex axis. Because no difference was found in the proportion of spiral trajectories between the different species (Table 3), the data were pooled and tested. The results showed an increase in the proportion of spiral trajectories with increased vortex strength for all species tested (Fig. 5a; $p < 0.001$). The maximum value of the proportion of spiral trajectories asymptotes at ~ 60% for all the copepod species.

Parameters that quantify the trajectory shape, such as NGDR, fractal dimension, and turn frequency, corroborate the increasingly curved and spiral shape of the trajectories with increased vortex strength (Fig. 5). These quantities exhibited a species dependence, which suggests that the species achieve the curved and spiral trajectory shapes via different methods. Although NGDR was significantly different among the species (Table 3), each species responded similarly to increased vortex strength by showing a decrease in their path NGDR (Fig. 5b). Similarly, there were significant interactive effects between species and vortex orientation ($p = 0.009$), and vortex orientation and axial strain rate ($p = 0.019$). For *A. tonsa* and *T. longicornis*, there was no significant effect of orientation of the vortex on

Table 3. Three-way ANOVA analysis of swimming kinematic variables for three species (*Acartia tonsa, Temora longicornis*, and *Calanus finmarchicus*), two vortex orientations (horizontal and vertical), and five vortex strengths as quantified by axial strain rate (s^{-1}) (stagnant flow control plus the four levels quantified in Table 2). The employed transformation is indicated for the kinematic variables that do not follow a normalized distribution.

		Proportion of spiral trajectories (%)	NGDR	Fractal dimension	Turn frequency (turns copepod^{-1} s^{-1})	Relative velocity (cm s^{-1})	Hop frequency (hops copepod^{-1} s^{-1})	Hop acceleration (cm s^{-2})	Escape frequency (escapes copepod^{-1} s^{-1})	Escape acceleration (cm s^{-2})	PRT	Trajectory angle with respect to local flow direction (°)	Escape angle with respect to gravity (°)
Transformation		SQRT	LN				LN	LN	LN	LN			
Species	d*F* (*x*,*y*)	(2,89)	(2,84)	(2,84)	(2,89)	(2,89)	(2,89)	(2,87)	(2,89)	(2,82)	(2,71)	(2,71)	(2,82)
	F	2.793	4.371	15.853	19.521	11.174	32.86	9.508	8.328	36.329	57.617	10.299	3.892
	p	0.069	0.017*	< 0.001*	< 0.001*	< 0.001*	< 0.001*	< 0.001*	< 0.001*	< 0.001*	< 0.001*	< 0.001*	0.002*
Orientation	d*F* (*x*,*y*)	(1,89)	(1,84)	(1,84)	(1,89)	(1,89)	(1,89)	(1,87)	(1,89)	(1,82)	(1,70)	(1,71)	(1,82)
	F	1.50	1.223	0.579	9.974	0.876	2.718	0.647	0.014	0.259	2.806	0.011	0.885
	p	0.225	0.274	0.450	0.002*	0.353	0.104	0.425	0.904	0.613	0.101	0.916	0.351
Axial strain rate (s^{-1})	d*F* (*x*,*y*)	(4,89)	(4,84)	(4,84)	(4,89)	(4,89)	(4,89)	(4,87)	(4,89)	(4,82)	(3,70)	(3,71)	(4,82)
	F	114.48	26.10	31.748	4.458	5.683	0.381	1.814	1.300	1.323	1.450	26.778	2.999
	p	< 0.001*	< 0.001*	< 0.001*	0.003*	< 0.001*	0.821	0.138	0.280	0.273	0.240	< 0.001*	0.002*
Species × orientation	d*F* (*x*,*y*)	(2,89)	(2,84)	(2,84)	(2,89)	(2,89)	(2,89)	(2,87)	(2,89)	(2,82)	(2,70)	(2,71)	(2,82)
	F	1.853	5.183	0.469	6.914	1.115	6.716	0.659	0.177	1.067	6.670	1.165	2.307
	p	0.166	0.009*	0.628	0.002*	0.335	0.002	0.521	0.838	0.351	0.003*	0.320	0.109
Species × axial strain rate	d*F* (*x*,*y*)	(8,89)	(8,84)	(8,84)	(8,89)	(8,89)	(8,89)	(8,87)	(8,89)	(8,82)	(6,70)	(6,71)	(8,82)
	F	1.332	1.612	3.936	0.786	1.7450	1.316	1.639	1.448	1.344	0.881	0.424	1.003
	p	0.245	0.143	< 0.001*	0.616	0.108	0.002*	0.134	0.196	0.243	0.516	0.859	0.445
Orientation × axial strain rate	d*F* (*x*,*y*)	(4,89)	(4,84)	(4,84)	(4,89)	(4,89)	(4,89)	(4,87)	(4,89)	(4,82)	(3,70)	(3,71)	(4,82)
	F	1.235	3.207	0.609	0.232	0.304	1.061	0.441	0.296	0.933	0.077	0.131	1.490
	p	0.306	0.019*	0.658	0.919	0.874	0.384	0.778	0.879	0.452	0.972	0.941	0.218
Species × orientation × axial strain rate	d*F* (*x*,*y*)	(8,89)	(8,84)	(8,84)	(8,89)	(8,89)	(8,89)	(8,87)	(8,89)	(8,82)	(6,70)	(6,71)	(8,82)
	F	1.540	1.503	1.062	0.919	1.121	1.097	1.032	0.748	0.111	0.347	0.185	1.168
	p	0.163	0.178	0.403	0.507	0.998	0.378	0.423	0.649	0.999	0.908	0.980	0.336

*$p < 0.05$.

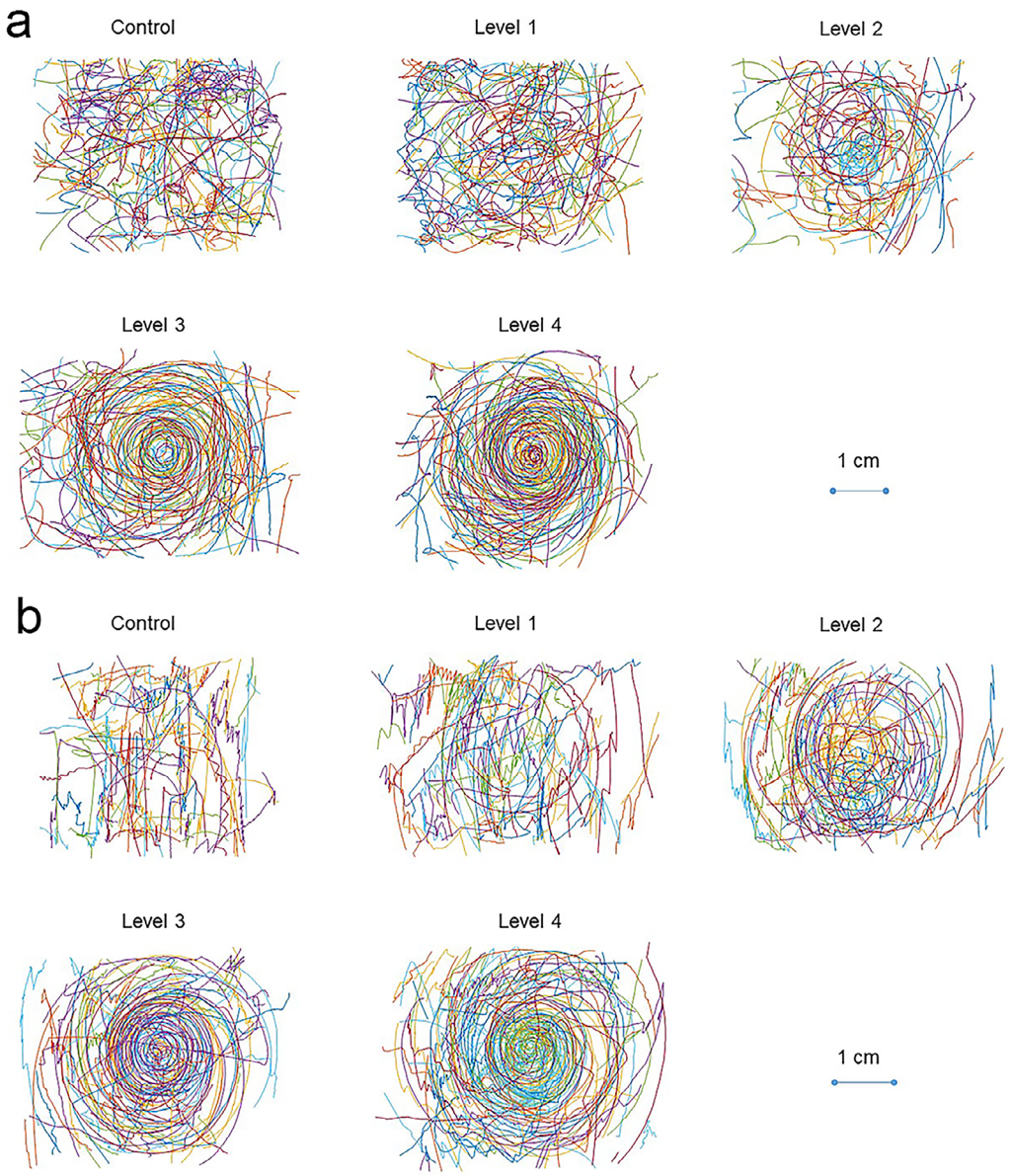

Fig. 4. Copepod trajectories. (**a**) *Temora longicornis* and (**b**) *Calanus finmarchicus* trajectories in the control and the four vortex treatments (from the disk view) in the horizontal apparatus. The colors represent different trajectories. Trajectories were recorded for the treatments sequenced in a random order, and different populations were used for each replicate. Each plot for *T. longicornis* includes between 71 and 125 trajectories, and each plot for *C. finmarchicus* includes between 73 and 103 trajectories, as quantified in Supporting Information (Table S1).

NGDR. As a result, NGDR at each axial strain rate was pooled for horizontal and vertical treatments (Fig. 5b). For both species, NGDR decreased linearly with increased vortex strength. In contrast, NGDR for *C. finmarchicus* showed a significant effect of vortex orientation and axial strain rate. Similar to the other two species, the regressions for *C. finmarchicus* with respect to axial strain rate revealed a significant decrease in NGDR with increased vortex strength, although the effect on the NGDR was more pronounced when the vortex was oriented in the horizontal direction (Fig. 5b). Mean values decreased from 0.36 ± 0.06 (mean ± SE; control) to 0.12 ± 0.02 (level 4) for *A. tonsa*, from 0.46 ± 0.21 (control) to 0.23 ± 0.10 (level 4) for *T. longicornis*, and from 0.46 ± 0.01 (control) to 0.19 ± 0.02 (level 4) for *C. finmarchicus* in the horizontal treatment, and from 0.27 ± 0.16 (control) to 0.15 ± 0.02 (level 4) for *C. finmarchicus* in the vertical treatment (Fig. 5b). The fractal dimension of the swimming paths showed no difference between horizontal and vertical orientations (Table 3). However, for all of the species, the fractal dimension increased with increased vortex strength (Fig. 5c). The turn frequency of the copepods differed significantly with vortex orientation (Table 3). When the vortex axis was horizontal, all three

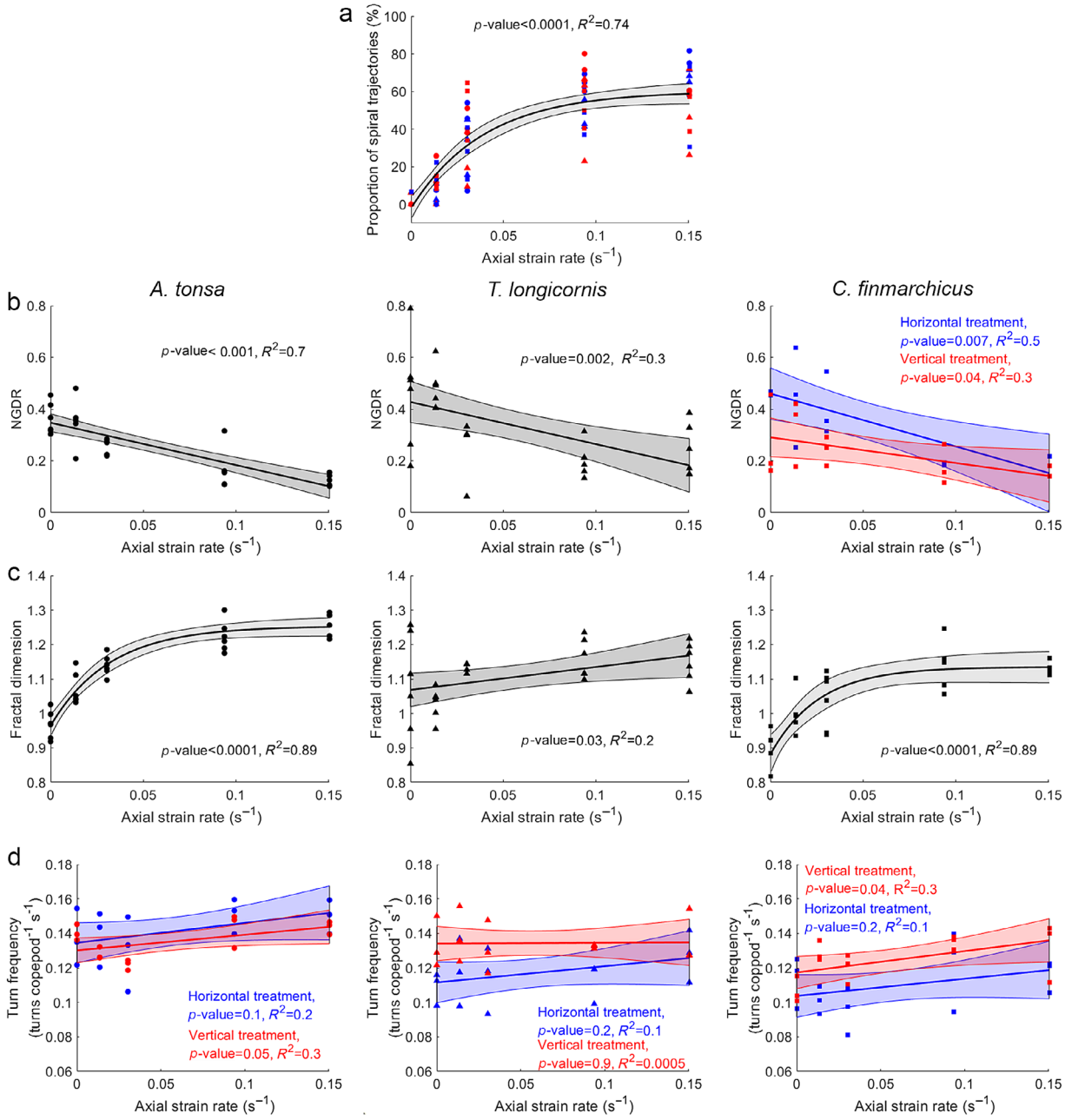

Fig. 5. Regression models of swimming kinematic parameters vs. vortex axial strain rate. (**a**) Proportion of spiral trajectories, (**b**) NGDR, (**c**) fractal dimension, and (**d**) turn frequency are presented for three species of *Acartia tonsa* (left, circle symbols), *Temora longicornis* (middle, triangle symbols), and *Calanus finmarchicus* (right, square symbols). Data shown in red correspond to the vertical vortex treatment and data shown in blue correspond to the horizontal vortex treatment. Data shown in gray were pooled for horizontal and vertical treatments. The shaded areas show the 95% confidence interval for the parameter. The *p*-value and R^2 of the statistical analysis are reported for each parameter. Non-linear regression was used for (**a**) and (**c**) (*A. tonsa* and *C. finmarchicus*). Calculated parameters for all regression equations are shown in Supporting Information (Table S2).

species tested showed no change in turn frequency with increased vortex intensity. However, when the vortex axis was oriented in the vertical direction, two of the copepod species (*A. tonsa* and *C. finmarchicus*) showed a small (< 10%), but significant, increase in turn frequency with increased vortex strength (Fig. 5d). *T. longicornis* showed no change in turn frequency with increased vortex strength (Fig. 5d).

Swimming kinematics were evaluated using the relative velocity, hop frequency, hop acceleration, escape frequency, and escape acceleration. Of these, only relative velocity and hop frequency showed any significant effect on the copepods tested (Table 3; effect of vortex strength and interactive effect of species × vortex strength, respectively). The relative swimming velocity for *A. tonsa* and *C. finmarchicus* increased with increased

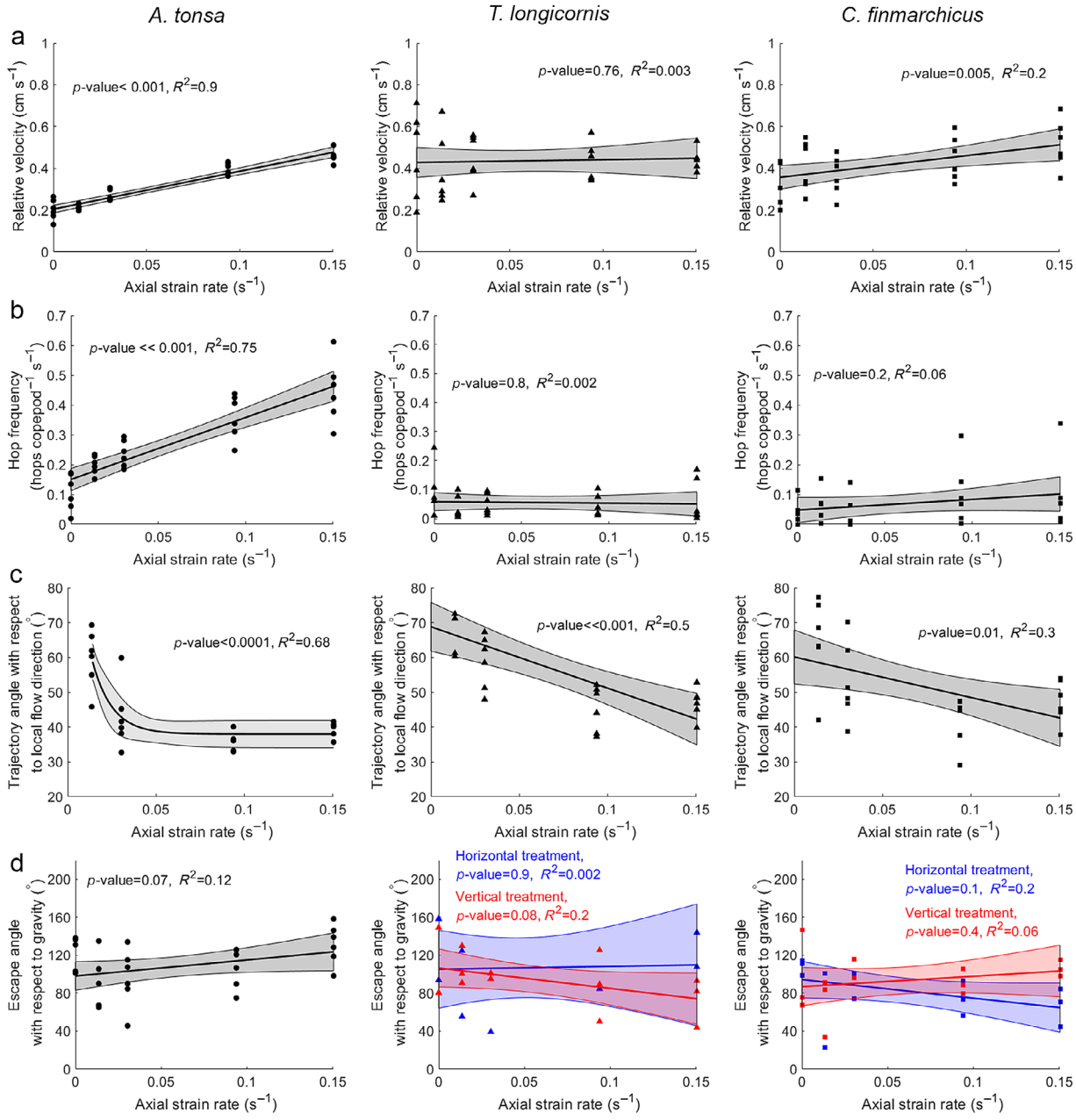

Fig. 6. Regression models of swimming kinematic parameters vs. vortex axial strain rate. (**a**) Relative velocity, (**b**) hop frequency, (**c**) trajectory angle with respect to local flow direction, and (**d**) escape angle with respect to gravity. *Acartia tonsa* (left, circle symbols), *Temora longicornis* (middle, triangle symbols), and *Calanus finmarchicus* (right, square symbols). Data shown in red correspond to the vertical vortex treatment and data shown in blue correspond to the horizontal vortex treatment. Data shown in gray were pooled for horizontal and vertical treatments. The shaded areas show the 95% confidence interval for the parameter. The *p*-value and R^2 of the statistical analysis are reported for each parameter. Non-linear regression was used for (**c**) (*A. tonsa*). Calculated parameters for all regression equations are shown in Supporting Information (Table S2).

vortex intensity (Fig. 6a) with no effect of vortex orientation. *A. tonsa* increased the relative velocity in response to the increased vortex strength by 125% (from 0.20 ± 0.04 cm s^{-1} in the control to 0.45 ± 0.08 cm s^{-1} at level 4). Similarly, *C. finmarchicus* showed an increase in relative swimming velocity with vortex strength from 0.34 ± 0.11 cm s^{-1} in control level to 0.52 ± 0.12 cm s^{-1} in level 4 (Fig. 6a). It is important to note that each copepod species employ a different swimming strategy to maintain a larger relative velocity with respect to the vortex flow. *C. finmarchicus* and *A. tonsa* are "cruise-sink" and "hop-sink" copepods, respectively, that punctuate their forward motion with brief periods of sinking. *A. tonsa* uses only its swimming legs during the hop, whereas *C. finmarchicus* uses a combination of its swimming legs and its cephalic

appendages to move forward. Although the speed of each hop is similar between the two species, the duration of elevated speed is much longer in *C. finmarchicus*. To travel a larger distance, *A. tonsa* rely on changes in the frequency of their jumps, whereas *C. finmarchicus* appears to increase the duration of the hop to modulate their speed. The hop frequency for *A. tonsa* increased from 0.10 ± 0.06 hops copepod^{-1} s^{-1} in the control to 0.44 ± 0.10 hops copepod^{-1} s^{-1} in level 4 with no effect of vortex orientation (Fig. 6b). In contrast, *C. finmarchicus* showed no significant change in hop frequency (Fig. 6b) despite an increase in the relative swimming speed with increased vortex strength (Fig. 6a). In contrast to the other species, *T. longicornis* showed no significant change in the relative velocity or hop frequency with either vortex strength or orientation (Fig. 6).

The mean trajectory angle with respect to the local flow direction varied significantly for species and axial strain rate, but was not affected by the vortex orientation (Table 3). For each species, the mean trajectory angle with respect to the local flow direction decreased with vortex strength (Fig. 6c) indicating copepod trajectories become more aligned with the local fluid motion as the proportion of spiral swimming paths increased. At the highest vortex intensity (level 4), the mean trajectory angle with respect to the local flow direction was $39.5^{\circ} \pm 2.2^{\circ}$ for *A. tonsa*, $46.9^{\circ} \pm 4.3^{\circ}$ for *T. longicornis*, and $47.3^{\circ} \pm 6.1^{\circ}$ for *C. finmarchicus* (Fig. 6c). Escape angle with respect to gravity was significantly different for species and axial strain rate with no interactive effects (Table 3). However, the regression models were not significant with respect to axial strain rate (Fig. 6d). Finally, no correlation was found between body axis orientation of *C. finmarchicus* and vortex strength. *C. finmarchicus* had an upward body orientation (i.e., body axis orientation angle with respect to the direction of gravity [i.e., down] is 118° to 152°) and the orientation was not affected by vortex strength.

To determine the fluid velocity gradient characteristics (i.e., hydrodynamic cue) that caused a hop or escape reaction in copepods, jump density at different radial positions within the vortex was calculated (Fig. 7). Species-specific responses are evident in the jump density profiles. *A. tonsa* showed the greatest jump density inside the vortex core and the jump density increased with increased vortex intensity in both the horizontal and vertical orientations (Fig. 7a). Because of the spatial co-occurrence between the location of maximum vorticity (*see* Fig. 3a) and location of the maximum jump density (Fig. 7a), Elmi et al. (2021) concluded that vorticity is the main hydrodynamic cue triggering jump response in *A. tonsa*. *T. longicornis*, in contrast, did not show any significant jumping behavior as a function of radial position and little or no change with vortex intensity (Fig. 7b). *C. finmarchicus* showed an intermediate jump response to the vortex. *C. finmarchicus* in the horizontal vortex orientation was similar to *T. longicornis* and showed no differential response to the location within the vortex or to increased intensity of the vortex. In contrast, when *C. finmarchicus* was exposed to the vortex in the vertical orientation, they responded similarly to that of *A. tonsa* with

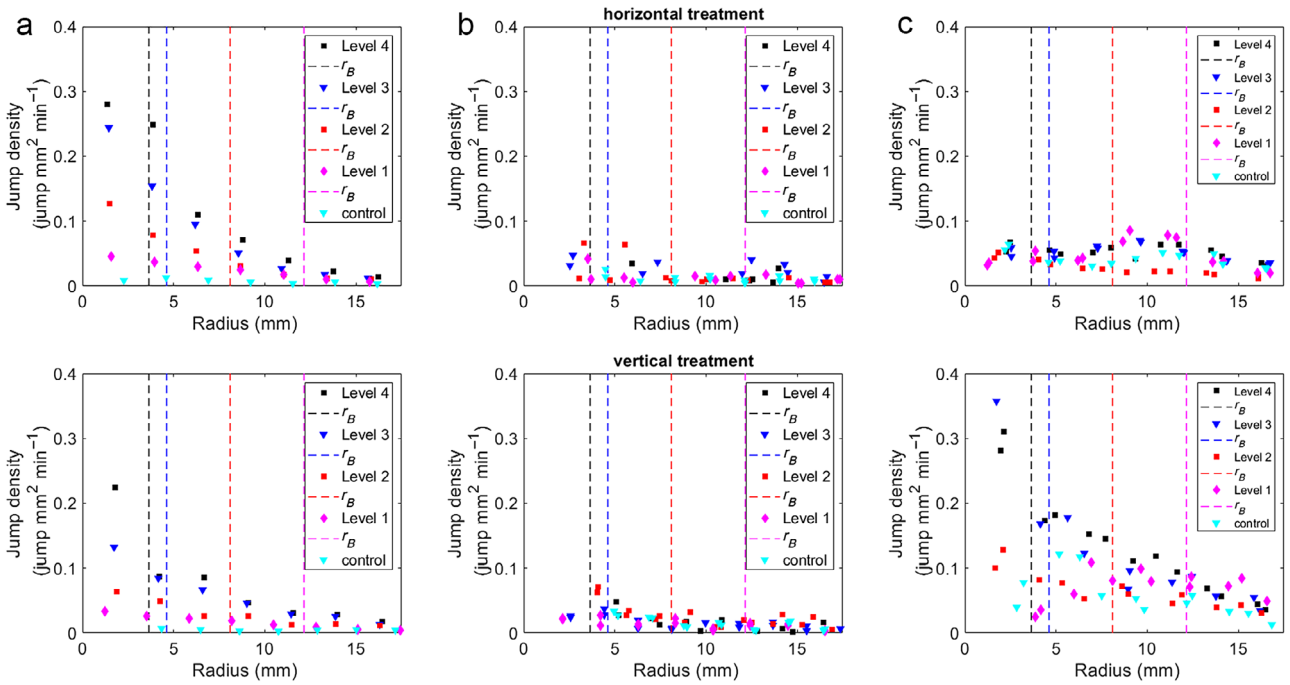

Fig. 7. Jump density as a function of distance from the vortex axis with constant bin width ($\Delta r = 1$ mm). (**a**) *Acartia tonsa*, (**b**) *Temora longicornis*, and (**c**) *Calanus finmarchicus* with the horizontal vortex treatment on the top row and vertical vortex treatment on the bottom row. The dashed lines represent the characteristic radius of the vortex (r_B) for each level.

increased jump density with vortex strength and greater number of jumps inside the vortex core (Fig. 7c). Thus, *C. finmarchicus* showed the strongest vortex orientation-dependent behaviors quantified in this study. Similar to the conclusion for *A. tonsa*, this suggests that the hydrodynamic cue triggering a jump response in *C. finmarchicus* is vorticity, but only in the vertical orientation of the vortex.

Discussion

Small-scale turbulence is an important driver of zooplankton population dynamics (Marrasé and Saiz 1997). Yet, little is known about the behavioral responses of individual copepods that mechanistically drive larger-scale population effects. At the scale of a copepod, turbulent fluid motion manifests as coherent vortices that dissipate kinetic energy. This study investigates the interaction of three copepod species with an isolated vortex structure that was varied in strength, size, and orientation to mimic a range of dissipation-scale turbulent eddies. The discussion that follows addresses similarities and differences of the main behavioral responses that emerge from the analysis and connects the findings to the swimming style and setal morphology of the copepod species examined.

Copepods detect the turbulent vortex

The results of this study clearly establish that marine copepods sense and respond to the flow structure of dissipation-scale turbulent eddies. All three copepod species altered the shape of their swimming trajectory in response to the vortex flow by transitioning from relatively straight trajectories to more curved and spiral trajectories as the intensity of the vortex increased. The swimming kinematics show a clear species-specific response, with *A. tonsa* and *C. finmarchicus* exhibiting the strongest behavioral response to increased vortex strength and *T. longicornis* exhibited the weakest response. In response to the Burgers vortex, the copepods rarely elicited an escape response as they do for siphon flow (Fields and Yen 1997; Kiørboe et al. 1999; Fields et al. 2012) and never showed indications of mate tracking (Weissburg et al. 1998) or an attack response (Fields and Yen 2002). Thus, the response of the copepods indicates that they can differentiate between the flow created by a turbulent vortex from the flows created by a predator, prey, or conspecific. Rather than escaping or avoiding the circular fluid motion of the vortex, an increasing percentage of all three copepod species moved in the direction of the flow, partially by flow advection and partially by active behavior.

A. tonsa move through the water via a combination of hops, escapes, and forward motion caused by their feeding current (Tiselius and Jonsson 1990). The increasing hop frequency with increased vortex strength is consistent with the findings that *A. tonsa* are highly mechanosensitive (Fields and Yen 1997; Kiørboe et al. 1999). *A. tonsa* possesses a three-dimensional array of setae on their antennules (Fig. 1a), which is particularly well suited to sensing velocity gradients with various orientations. Keep in mind that vorticity physically represents the local velocity gradients that describe rotation of the fluid. Hence, in the vortex core where the vorticity is large, the three-dimensional sensory array of *A. tonsa* is advantageous for detecting the local hydrodynamic cue. The lack of a similar response in *T. longicornis* suggests that its planar setal array is less suited to sense the velocity gradients associated with vorticity. *C. finmarchicus* provides a fascinating set of behaviors. *C. finmarchicus* did not increase hop or escape frequency with increased vortex strength; however, when they jumped, the events were stronger and longer distance than the other species. The increased jump density for *C. finmarchicus* in the vortex core only for the vertical treatment may be due to the body orientation during sinking, which could place the planar setal array in an orientation to detect the fluid vorticity when the vortex is vertically oriented, but not when the vortex is horizontally oriented. *C. finmarchicus* had an upward body axis orientation, and the body axis orientation was not affected by vortex strength.

Small-scale dissipative eddies aggregate copepods

Once within the vortex, copepods moved faster and in the same direction as the prevailing flow. The results for *C. finmarchicus* and *T. longicornis* are consistent with Elmi et al. (2021), which focused on the estuarine copepod *A. tonsa*. Together these data indicate that movement in the direction of the vortex flow may be a common behavioral trait among copepods, although each species appears to employ unique mechanisms to achieve it. For example, *A. tonsa* followed the local fluid velocity closely, except for the intermittent hops and escapes (Fig. 8a, also *see* Elmi et al. 2021). When *A. tonsa* hopped or escaped, it moved the copepod across streamlines (both inward and outward). The combination of randomly directed hops and inward advection by the rotating Burgers vortex flow gradually moved the copepod radially inward toward the vortex core (Fig. 8a). As the copepod approached the core, the frequency of hopping increased and the rate of approach increased causing the copepod to be retained near the center of the Burgers vortex. The pattern of aggregating toward the core of the vortex was similar for *T. longicornis*, but the behavioral mechanism driving the process was quite different. *T. longicornis* showed no changes in the number of hops or escapes in response to the vortex strength or orientation; however, they did increase their swimming speed in the direction of the fluid motion (Fig. 8b). As *T. longicornis* increased their swimming speed, it exceeded the local fluid velocity. The elevated speed, in addition to the swimming angle, propelled the copepod faster and steered them toward the center of the vortex. The example trajectory of *C. finmarchicus* (Fig. 8c) was similar to those of *A. tonsa* in some ways, but also demonstrated differences. Similar to *A. tonsa*, *C. finmarchicus* hopped during its normal swimming behavior. Although the hop frequency did not increase in response to the vortex intensity (in contrast to *A. tonsa*), the hop duration (and distance) was greater compared to the hops

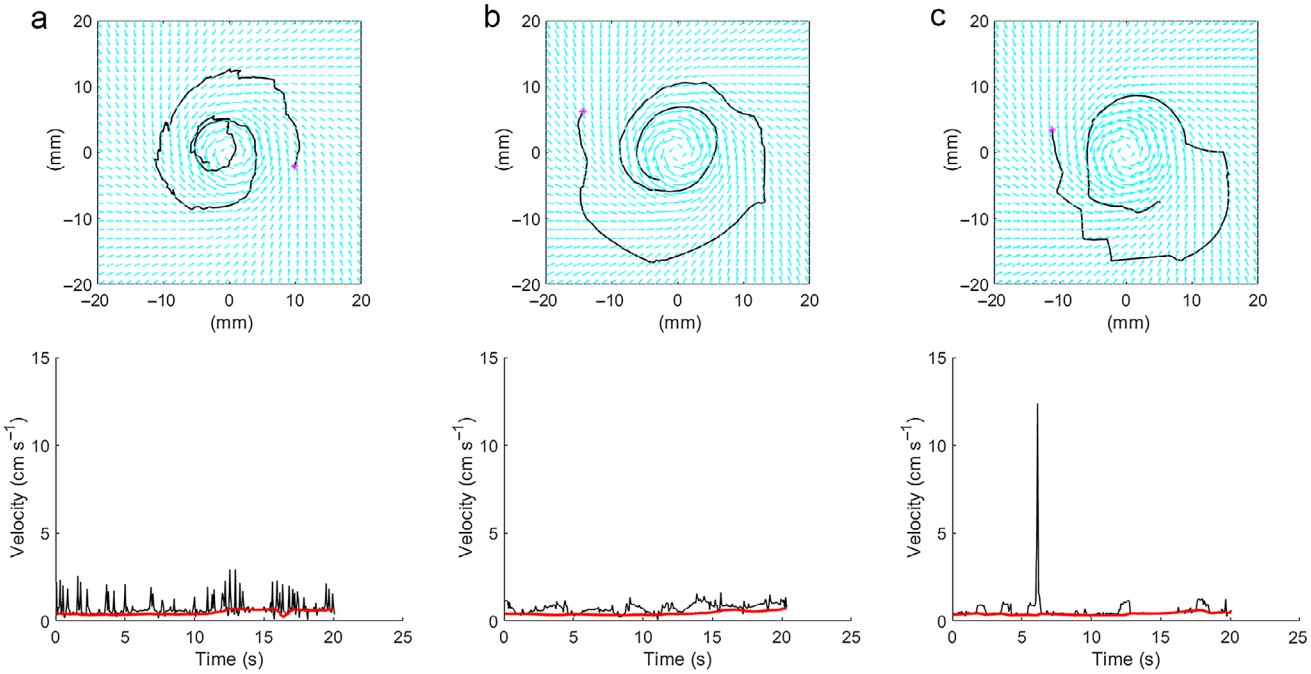

Fig. 8. Example spiral trajectories in the level 4 vortex treatment with the corresponding time record of copepod velocity shown in black. The time record of fluid velocity at the copepod position is shown in red. In the trajectory plots, the starting location is marked with a pink dot and the fluid rotation and copepod trajectory are in the counterclockwise sense of rotation. (**a**) *Acartia tonsa*, (**b**) *Temora longicornis*, and (**c**) *Calanus finmarchicus*.

of *A. tonsa*. The effect of the longer-displacement hops and escape events was to move the copepod across streamlines (both inward and outward) causing a jagged spiral trajectory (Fig. 8c).

Due to the observed greater relative velocity, the copepods increase their encounter rate with food and with conspecifics. A higher relative velocity also agrees with previous studies showing higher metabolic rates in turbulent flows (Saiz and Alcaraz 1992; Alcaraz et al. 1994). While previous studies have shown that turbulence increases the encounter rate with potential mates and food items through flow enhanced contact rates (Rothschild and Osborn 1988; Michalec et al. 2020), this study found that increased encounter rates is, in part, the result of advection due to turbulent fluid motion and increased copepod swimming speed (either via jumps or cruising). It is important to note that the assumption that copepod swimming speed is largely independent of the turbulent fluid motion, and is therefore additive when computing relative velocity, is not correct in a dissipative-scale turbulent eddy. By moving with the fluid motion in a turbulent eddy, the relative velocity of the copepod and adjacent objects is smaller than is often assumed.

The pattern and shape of the trajectories for all three copepod species show that the copepods are retained in the Burgers vortex for longer than if they simply continued along their relatively straight trajectories. These results suggest that the fluid motion in the Burgers vortex combined with copepod behavioral responses cause copepods to aggregate into higher density patches (Elmi et al. 2021). These high-density patches may benefit copepods due to the enhance encounter rates between conspecifics (Michalec et al. 2020) or conceal the copepods feeding current from other mechanoreceptive predators (Fields 1996). Alternatively, the aggregations may provide localized feeding grounds for visual predators such as larval fish. Prey aggregation plays a vital role in ocean food web ecology (Olson and Backus 1985; Flierl and Woods 2015). Copepods are known to aggregate in larger-scale fluid features such as upwelling and downwelling regions along ocean fronts (Wishner et al. 1995; Sims and Quayle 1998; Werner et al. 2003). Zooplankton aggregation often involves a combination of fluid physics and individual behavior (Flierl et al. 1999; Genin et al. 2005; True et al. 2015). The patches combined with the higher encounter rates due to increased turbulent velocity (Rothschild and Osborn 1988) may help to resolve the paradox between the high concentrations of food needed to sustain fish larvae in the lab and the low average concentrations found in the field (Lasker 1981).

Response to vortex orientation

It is well known that copepods show neurophysiological and behavioral responses to fluid flow signals (Yen et al. 1992). Previous work has shown that individual mechanosensors on the antennules of the copepod have directional sensitivity to hydrodynamic cues (Fields et al. 2002). The ability to detect flow direction allows the copepod to orient to potential prey in three-dimensional space (Doall et al. 2002) and to escape when they are approached by a

predator from different directions (Fields and Yen 1997; Fields 2010; Fields et al. 2012). Although all three species of copepods responded to the vortex, the responses to the orientation of the vortex were not consistent among the species. Only turn frequency was affected by the vortex orientation for all three copepod species examined. Slight differences in the response to vortex orientation were noted in NGDR for *C. finmarchicus*. These results are consistent with the response of *C. finmarchicus* to a siphon flow where the copepods escaped at different distances depending on their orientation to the flow (Fields et al. 2012). Notably, *A. tonsa* showed the same response to the vortex in each orientation. This is intriguing given the difference in escape thresholds due to orientation in response to a siphon flow (Fields 2010). One explanation might be that the siphon flow mimics a predator and the copepods respond with a clear directional escape. In contrast, the vortex is an environmental feature and *A. tonsa* may have no ecological reason to behave differently based on vortex orientation. In either orientation, the turbulent eddy flow structure may increase the copepod's encounter rate with food and conspecifics.

Sensory and vertical distribution considerations

A key conclusion of this work is that copepods respond to turbulent vortex structure at dissipative scales. Although the frequency and orientation of dissipative-scale eddies in the ocean are not quantified, they are likely to be numerous, relatively long lived (tens of seconds), and oriented in random directions (Yamazaki 1993; Webster et al. 2004; Jumars et al. 2009). The open ocean is generally less turbulent than tidal estuaries, and as such, open-ocean copepods are not likely to have evolved to exploit the high-intensity features created in this study. Similarly, both *T. longicornis* and *C. finmarchicus* possess planar setal arrays that are not likely to be equally sensitive to the vortex flow in all orientations. Both species showed a muted response to the vortex treatments. These results suggest that they are less likely to be able to fully exploit the vortex in all orientations and intensities. In contrast, *A. tonsa* is a dominant estuary species that experiences relatively high levels of turbulence. They responded to the Burgers vortex in both the horizontal and vertical orientations and showed an increase in their behavior response with increased vortex intensity. High-sensitivity and omnidirectional response may be the result of *A. tonsa* three-dimensional setal array arrangement. Although speculative, *A. tonsa* may exploit these small flow features to find food, encounter mates, and conceal their hydrodynamic signals from predators, thereby reducing the risk of being captured (Jiang and Kiørboe 2011).

The selection of vertical position in the water column undoubtedly is influenced by many factors, including food availability, individual feeding modes, predation risk, temperature, and light level (Tiselius and Jonsson 1990; Mackas et al. 1993). Despite the known importance of turbulence to vital rate functions (i.e., feeding, respiration, and reproduction) and trophic interactions, understanding the effects of turbulence is still in its infancy. It is intriguing to speculate on the correlation between turbulence level and the vertical (and horizontal) distribution of copepods. And, there is clear evidence that vertical distribution patterns of copepod species correlate to the turbulent energy dissipation rate (Mackas et al. 1993; Lagadeuc et al. 1997; Incze et al. 2001). The interaction between small-scale turbulent flow structure, as in this study, and the vital functions of these small organisms warrants closer scrutiny under varied conditions.

Data availability statement

Data are available from BCO-DMO (project URL https://www.bco-dmo.org/project/653235): doi:10.26008/1912/bco-dmo.834530.1 and doi:10.26008/1912/bco-dmo.818213.1

References

Alcaraz, M., and E. Saiz. 1992. External energy and plankton: New insights on the role of small-scale turbulence on zooplankton ecology. Oecol. Aquatic **10**: 137–144.

Alcaraz, M., E. Saiz, and A. Calbet. 1994. Small-scale turbulence and zooplankton metabolism: Effects of turbulence on heartbeat rates of planktonic crustaceans. Limnol. Oceanogr. **39**: 1465–1470. doi:10.4319/lo.1994.39.6.1465

Bagøien, E., and T. Kiørboe. 2005. Blind dating—Mate finding in planktonic copepods. III. Hydromechanical communication in *Acartia tonsa*. Mar. Ecol. Prog. Ser. **300**: 129–133. doi:10.3354/meps300129

Beaugrand, G., K. M. Brander, J. A. Lindley, S. Souissi, and P. C. Reid. 2003. Plankton effect on cod recruitment in the North Sea. Nature **426**: 661–664. doi:10.1038/nature02164

Burdick, D. S., D. K. Hartline, and P. H. Lenz. 2007. Escape strategies in co-occurring calanoid copepods. Limnol. Oceanogr. **52**: 2373–2385. doi:10.4319/lo.2007.52.6.2373

Burgers, J. M. 1948. A mathematical model illustrating the theory of turbulence. Adv. Appl. Mech. **1**: 171–199. doi:10.1016/S0065-2156(08)70100-5

Castonguay, M., S. Plourde, D. Robert, J. A. Runge, and L. Fortier. 2008. Copepod production drives recruitment in a marine fish. Can. J. Fish. Aquat. Sci. **65**: 1528–1531. doi:10.1139/F08-126

Doall, M. H., J. R. Strickler, D. M. Fields, and J. Yen. 2002. Mapping the free-swimming attack volume of a planktonic copepod, *Euchaeta rimana*. Mar. Biol. **140**: 871–879. doi:10.1007/s00227-001-0735-z

Elmi, D., D. R. Webster, and D. M. Fields. 2021. Response of the copepod *Acartia tonsa* to the hydrodynamic cues of small-scale, dissipative eddies in turbulence. J. Exp. Biol. **224**: jeb237297. doi:10.1242/jeb.237297

Fields, D. M. 1996. The interaction of calanoid copepods with a moving fluid environment: Implications for the role of

feeding current morphology in predator-prey interactions. Ph.D. Thesis. State Univ. of New York, Stony Brook, p. 353.

Fields, D. M. 2000. Characteristics of the high frequency escape reactions of *Oithona* sp. Mar. Freshw. Behav. Physiol. **34**: 21–35. doi:10.1080/10236240009379057

Fields, D. M. 2010. Orientation affects the sensitivity of *Acartia tonsa* to fluid mechanical signals. Mar. Biol. **157**: 505–514. doi:10.1007/s00227-009-1336-5

Fields, D. M. 2014. The sensory horizon of marine copepods, p. 157–179. *In* L. Seuront [ed.], Copepods: Diversity, habitat, and behavior. Nova Publishers.

Fields, D. M., D. S. Shaeffer, and M. J. Weissburg. 2002. Mechanical and neural responses from the mechanosensory hairs on the antennule of *Gaussia princeps*. Mar. Ecol. Prog. Ser. **227**: 173–186. doi:10.3354/meps227173

Fields, D. M., and J. Yen. 1997. The escape behavior of marine copepods in response to a quantifiable fluid mechanical disturbance. J. Plankton Res. **19**: 1289–1304. doi:10.1093/plankt/19.9.1289

Fields, D. M., and J. Yen. 2002. Fluid mechanosensory stimulation of behaviour from a planktonic marine copepod *Euchaeta rimana* Bradford. J. Plankton Res. **24**: 747–755. doi:10.1093/plankt/24.8.747

Fields, D. M., S. D. Shema, H. I. Browman, T. Q. Browne, and A. B. Skiftesvik. 2012. Light primes the escape response of the calanoid copepod, *Calanus finmarchicus*. PLoS One **7**: e39594. doi:10.1371/journal.pone.0039594

Flierl, G., D. Grunbaum, S. Levin, and D. Olson. 1999. From individuals to aggregations: The interplay between behavior and physics. J. Theor. Biol. **196**: 397–454. doi:10.1006/jtbi.1998.0842

Flierl, G. R., and N. W. Woods. 2015. Copepod aggregations: Influences of physics and collective behavior. J. Stat. Phys. **158**: 665–698. doi:10.1007/s10955-014-1162-0

Genin, A., J. S. Jaffe, R. Reef, C. Richter, and P. J. S. Franks. 2005. Swimming against the flow: A mechanism of zooplankton aggregation. Science **308**: 860–862. doi:10.1126/science.1107834

Haury, L. R., H. Yamazaki, and E. C. Itsweire. 1990. Effects of turbulent shear flow on zooplankton distribution. Deep Sea Res. A **37**: 447–461. doi:10.1016/0198-0149(90)90019-R

Hedrick, T. L. 2008. Software techniques for two-and three-dimensional kinematic measurements of biological and biomimetic systems. Bioinspir. Biomim. **3**: 034001. doi:10.1088/1748-3182/3/3/034001

Incze, L. S., D. Hebert, N. Wolff, N. Oakey, and D. Dye. 2001. Changes in copepod distributions associated with increased turbulence from wind stress. Mar. Ecol. Prog. Ser. **213**: 229–240. doi:10.3354/meps213229

Jiang, H., and T. Kiørboe. 2011. Propulsion efficiency and imposed flow fields of a copepod jump. J. Exp. Biol. **214**: 476–486. doi:10.1242/jeb.049288

Jumars, P. A., J. H. Trowbridge, E. Boss, and L. Karp-Boss. 2009. Turbulence-plankton interactions: A new cartoon. Mar. Ecol. Evol. Perspect. **30**: 133–150. doi:10.1111/j.1439-0485.2009.00288.x

Kiørboe, T., and E. Saiz. 1995. Planktivorous feeding in calm and turbulent environments, with emphasis on copepods. Mar. Ecol. Prog. Ser. **122**: 135–145. doi:10.3354/meps122135

Kiørboe, T., E. Saiz, and A. Visser. 1999. Hydrodynamic signal perception in the copepod *Acartia tonsa*. Mar. Ecol. Prog. Ser. **179**: 97–111. doi:10.3354/meps179097

Lagadeuc, Y., M. Boule, and J. J. Dodson. 1997. Effect of vertical mixing on the vertical distribution of copepods in coastal waters. J. Plankton Res. **19**: 1183–1204. doi:10.1093/plankt/19.9.1183

Lasker, R. [ed.]. 1981. Marine fish larvae. Morphology, ecology and relation to fisheries. Univ. of Washington Press.

Mackas, D. L., H. Sefton, C. B. Miller, and A. Raich. 1993. Vertical habitat partitioning by large calanoid copepods in the oceanic subarctic Pacific during Spring. Prog. Oceanogr. **32**: 259–294. doi:10.1016/0079-6611(93)90017-8

Manning, C. A., and A. Bucklin. 2005. Multivariate analysis of the copepod community of near-shore waters in the western Gulf of Maine. Mar. Ecol. Prog. Ser. **292**: 233–249. doi:10.3354/meps292233

Marrasé, C., J. H. Costello, T. Granata, and J. R. Strickler. 1990. Grazing in a turbulent environment: Energy dissipation, encounter rates, and efficacy of feeding currents in *Centropages hamatus*. Proc. Nat. Acad. Sci. USA **87**: 1653–1657. doi:10.1073/pnas.87.5.1653

Marrasé, C., E. Saiz, and J. M. Redondo [eds.]. 1997. Lectures on plankton and turbulence. Sci. Mar. **61**: 1–238.

Michalec, F.-G., I. Fouxon, S. Souissi, and M. Holzner. 2017. Zooplankton can actively adjust their motility to turbulent flow. Proc. Nat. Acad. Sci. USA **114**: E11199–E11207. doi:10.1073/pnas.1708888114

Michalec, F.-G., I. Fouxon, S. Souissi, and M. Holzner. 2020. Efficient mate finding in planktonic copepods swimming in turbulence. eLife **9**: e62014. doi:10.7554/eLife.62014

Murphy, D. W., D. R. Webster, and J. Yen. 2012. A high-speed tomographic PIV system for measuring zooplanktonic flow. Limnol. Oceanogr. Methods **10**: 1096–1112. doi:10.4319/lom.2012.10.1096

Olson, D. B., and R. H. Backus. 1985. The concentrating of organisms at fronts: A cold-water fish and a warm-core Gulf Stream ring. J. Mar. Res. **43**: 113–137. doi:10.1357/002224085788437325

Rothschild, B. J., and T. R. Osborn. 1988. Small-scale turbulence and plankton contact rates. J. Plankton Res. **10**: 465–474. doi:10.1093/plankt/10.3.465

Saiz, E. 1994. Observations of the free-swimming behavior of *Acartia tonsa*: Effects of food concentration and turbulent water motion. Limnol. Oceanogr. **39**: 1566–1578. doi:10.4319/lo.1994.39.7.1566

Saiz, E., and M. Alcaraz. 1992. Enhanced excretion rates induced by small-scale turbulence in *Acartia* (Copepoda:

Calanoida). J. Plankton Res. **14**: 681–689. doi:10.1093/plankt/14.5.681

Saiz, E., M. Alcaraz, and G. A. Paffenhöfer. 1992. Effects of small-scale turbulence on feeding rate and gross-growth efficiency of three Acartia species (Copepoda: Calanoida). J. Plankton Res. **14**: 1085–1097. doi:10.1093/plankt/14.8.1085

Saiz, E., and T. Kiørboe. 1995. Predatory and suspension feeding of the copepod *Acartia tonsa* in turbulent environments. Mar. Ecol. Prog. Ser. **122**: 147–158. doi:10.3354/meps122147

Seuront, L., J. S. Hwang, L. C. Tseng, F. G. Schmitt, S. Souissi, and C. K. Wong. 2004. Individual variability in the swimming behavior of the sub-tropical copepod *Oncaea venusta* (Copepoda: Poecilostomatoida). Mar. Ecol. Prog. Ser. **283**: 199–217. doi:10.3354/meps283199

Sims, D. W., and V. A. Quayle. 1998. Selective foraging behaviour of basking sharks on zooplankton in a small-scale front. Nature **393**: 460–464. doi:10.1038/30959

Tiselius, P. 1992. Behavior of *Acartia tonsa* in patchy food environments. Limnol. Oceanogr. **37**: 1640–1651. doi:10.4319/lo.1992.37.8.1640

Tiselius, P., and P. R. Jonsson. 1990. Foraging behavior of six calanoid copepods: Observations and hydrodynamic analysis. Mar. Ecol. Prog. Ser. **66**: 23–33. doi:10.3354/meps066023

True, A. C., D. R. Webster, M. J. Weissburg, J. Yen, and A. Genin. 2015. Patchiness and depth-keeping of copepods in response to simulated frontal flows. Mar. Ecol. Prog. Ser. **539**: 65–76. doi:10.3354/meps11472

Turner, J. T. 2004. The importance of small planktonic copepods and their roles in pelagic marine food webs. Zool. Stud. **43**: 255–266.

Vincent, A., and M. Meneguzzi. 1991. The spatial structure and statistical properties of homogeneous turbulence. J. Fluid Mech. **225**: 1–20. doi:10.1017/S0022112091001957

Visser, A. W., H. Saito, E. Saiz, and T. Kiørboe. 2001. Observations of copepod feeding and vertical distribution under natural turbulent conditions in the North Sea. Mar. Biol. **138**: 1011–1019. doi:10.1007/s002270000520

Waggett, R. J., and E. J. Buskey. 2007. Copepod escape behavior in non-turbulent and turbulent hydrodynamic regimes. Mar. Ecol. Prog. Ser. **334**: 193–198. doi:10.3354/meps334193

Webster, D. R., A. Brathwaite, and J. Yen. 2004. A novel laboratory apparatus for simulating isotropic oceanic turbulence at low Reynolds number. Limnol. Oceanogr. Methods **2**: 1–12. doi:10.4319/lom.2004.2.1

Webster, D. R., and D. L. Young. 2015. A laboratory realization of the Burgers' vortex cartoon of turbulence-plankton interactions. Limnol. Oceanogr. Methods **13**: 92–102. doi:10.1002/lom3.10010

Webster, D. R., D. L. Young, and J. Yen. 2015. Copepods' response to Burgers' vortex: Deconstructing interactions of copepods with turbulence. Integr. Comp. Biol. **55**: 706–718. doi:10.1093/icb/icv054

Weissburg, M. J., M. H. Doall, and J. Yen. 1998. Following the invisible trail: Kinematic analysis of mate-tracking in the copepod *Temora longicornis*. Philos. Trans. R. Soc. Lond. B Biol. Sci. **353**: 701–712. doi:10.1098/rstb.1998.0236

Werner, S. R., R. C. Beardsley, S. J. Lentz, D. L. Hebert, and N. S. Oakey. 2003. Observations and modeling of the tidal bottom boundary layer on the southern flank of Georges Bank. J. Geophys. Res. Oceans **108**: 8005. doi:10.1029/2001JC001271

Wishner, K. F., J. R. Schoenherr, R. Beardsley, and C. S. Chen. 1995. Abundance, distribution and population structure of the copepod *Calanus finmarchicus* in a springtime right whale feeding area in the southwestern Gulf of Maine. Cont. Shelf Res. **15**: 475–507. doi:10.1016/0278-4343(94)00057-T

Woodson, C. B., D. R. Webster, and A. C. True. 2014. Copepod behavior: Oceanographic cues, distributions, and trophic interactions, p. 215–253. *In* L. Seuront [ed.], Copepods: Diversity, habitat, and behavior. Nova Publishers.

Yamazaki, H. 1993. Lagrangian study of plankton organisms: Perspectives. Bull. Mar. Sci. **53**: 265–278.

Yen, J., P. H. Lenz, D. V. Gassie, and D. K. Hartline. 1992. Mechanoreception in marine copepods: Electrophysiological studies on the first antennae. J. Plankton Res. **14**: 495–512. doi:10.1093/plankt/14.4.495

Yokokawa, M., K. Itakura, A. Uno, T. Ishihara, and Y. Kaneda. 2002. 16.4-Tflops direct numerical simulation of turbulence by a Fourier spectral method on the Earth Simulator, p. 1–17. *In* Proceedings of the 2002 ACM/IEEE Conference on Supercomputing. IEEE Computer Society Press. doi:10.5555/762761.762808

Acknowledgments

The authors thank Shantanu Soumya, Yoonsoo Nam, Savannah Howard, Samantha Bennett, Dominique Howard, Agam Singh, and Tara Boyd for help with digitalization of the copepod tracks. Thanks also to Dr. Jeannette Yen for inspiration and early discussions. Funding was provided by U.S. National Science Foundation, Grants OCE-1537284 and OCE-1537579.

Conflict of Interest

None declared.

Submitted 21 July 2021
Revised 14 February 2022
Accepted 22 May 2022

Associate editor: Michael R. Stukel